

Quantized Andreev conductance in semiconductor nanowires

Yichun Gao,^{1,*} Wenyu Song,^{1,*} Yuhao Wang,^{1,*} Zuhan Geng,^{1,*} Zhan Cao,^{2,*} Zehao Yu,¹ Shuai Yang,¹ Jiaye Xu,¹ Fangting Chen,¹ Zonglin Li,¹ Ruidong Li,¹ Lining Yang,¹ Zhaoyu Wang,¹ Shan Zhang,¹ Xiao Feng,^{1,2,3,4} Tiantian Wang,^{2,4} Yunyi Zang,^{2,4} Lin Li,² Dong E. Liu,^{1,2,3,4} Runan Shang,^{2,4} Qi-Kun Xue,^{1,2,3,4,5} Ke He,^{1,2,3,4,†} and Hao Zhang^{1,2,3,‡}

¹State Key Laboratory of Low Dimensional Quantum Physics,

Department of Physics, Tsinghua University, Beijing 100084, China

²Beijing Academy of Quantum Information Sciences, Beijing 100193, China

³Frontier Science Center for Quantum Information, Beijing 100084, China

⁴Hefei National Laboratory, Hefei 230088, China

⁵Southern University of Science and Technology, Shenzhen 518055, China

Clean one-dimensional electron systems can exhibit quantized conductance. The plateau conductance doubles if the transport is dominated by Andreev reflection. Here, we report quantized conductance observed in both Andreev and normal-state transports in PbTe-Pb and PbTe-In hybrid nanowires. The Andreev plateau is observed at $4e^2/h$, twice of the normal plateau value of $2e^2/h$. In comparison, Andreev conductance in the best-optimized III-V nanowires is non-quantized due to mode-mixing induced dips (a disorder effect), despite the quantization of normal-state transport. The negligible mode mixing in PbTe hybrids indicates an unprecedented low-disorder transport regime for nanowire devices, beneficial for Majorana researches.

Superconductor-semiconductor hybrid nanowires have been extensively studied for over a decade as promising candidates for the realization of Majorana zero modes [1–11]. Despite significant progress in material growth and device control [12–15], current experiments remain limited by disorder. Disorder is also the key source of ongoing debates [16–23]. Even the highest-quality nanowires, after a decade of optimization, still cannot meet the stringent low-disorder requirement for topological Majoranas [24]. Therefore, further reducing disorder is urgently needed to advance this field and to settle the debates.

A direct assessment of disorder in a nanowire device is through the observation of quantized conductance, a hallmark of ballistic (quasi) one-dimensional electron systems. In the early nanowire experiments around 2012, devices were highly disordered, and quantized conductance was absent at zero magnetic field. Later on, improvements in device fabrication have enabled the observation of zero-field quantized plateaus in units of $2e^2/h$ in InSb and InAs devices configured in an N-NW-N geometry, where N stands for normal metal and NW for nanowire [25–27].

This quantization is also observed in the normal-state conductance of N-NW-S hybrid devices [28], where S stands for superconductor. The normal-state conductance, G_N , is measured by applying a bias voltage significantly larger than the superconducting gap. The Andreev conductance (G_S), on the other hand, is measured for biases within the gap. In the tunneling regime, G_S is suppressed relative to G_N , but it is enhanced in the open regime, i.e. the region of the G_N plateau. This enhancement is due to Andreev reflection, wherein an injected

electron is Andreev reflected as a hole, effectively doubling the charge transfer. Experimentally, this enhancement is rarely quantized due to significant fluctuations. In some regions on the G_N plateau, the enhancement factor can reach the doubling limit, i.e. $G_S \sim 4e^2/h$ [28–30], indicating a unity junction transmission (T) of Andreev process in those regions [31]. The enhancement in G_S is non-uniform and accompanied by large fluctuations, making it difficult to categorize as an Andreev plateau at $4e^2/h$. The reason for this is that G_S scales with T^2 , which is much more sensitive to disorder compared to G_N which scales with T . When the second channel begins to be occupied, disorder-induced mode-mixing can suppress G_S , resulting in a dip feature. In contrast, G_N is barely affected as the total transmission of the two channels remains unchanged. This disorder-induced dip, also revealed in numerical simulations [28, 32], is ubiquitous in the best-optimized III-V devices [28–30], preventing the formation of an Andreev plateau. While quantized Andreev conductance has long been predicted for clean N-NW-S devices [32, 33], it has yet to be observed in nanowire experiments.

Here, we report the observation of quantized Andreev conductance in PbTe nanowires coupled to superconductors Pb and In. At zero magnetic field, G_N is quantized at $2e^2/h$, exhibiting a diamond shape in the bias-gate 2D scan. The Andreev conductance is quantized at $4e^2/h$ without the mode-mixing-induced dip. At finite fields, superconductivity is suppressed, and the Andreev plateau transitions from $4e^2/h$ to $2e^2/h$. Our results suggest that transport in PbTe-Pb and PbTe-In nanowires achieves an unprecedented low-disorder regime compared to InAs and InSb nanowires. Given that PbTe has recently been proposed as a promising Majorana candidate, with rapid experimental advancements [34–48], these low-disorder hybrid nanowires may facilitate

* equal contribution

† kehe@tsinghua.edu.cn

‡ hzquantum@mail.tsinghua.edu.cn

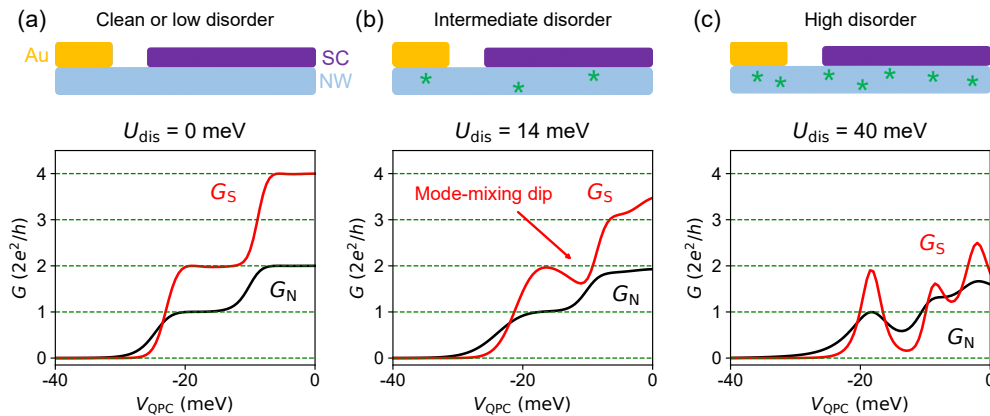


FIG. 1. Categorization of device disorder. (a) Clean or low disorder regime. Upper, N-NW-S (yellow-blue-violet) device schematic. Lower panel, transport simulation: Both G_S and G_N exhibit quantized plateaus. V_{QPC} refers the electrostatic potential of the barrier region, equivalent to a gate voltage. (b) Intermediate disorder regime. The green stars represent disorder for illustration purpose (not to scale). Lower panel, simulation reveals G_N plateau, while the G_S quantization is destroyed. The red arrow marks the characteristic dip induced by mode-mixing. (c) High disorder regime (illustrated as more green stars) with no quantization in either G_S or G_N . Magnetic field is zero for the simulations.

cleaner Majorana experiments in future research.

Figure 1 shows schematics of N-NW-S devices and numerical simulations of transport under varying disorder conditions. We categorize the disorder levels into three regimes: clean or low disorder (Fig. 1(a)), intermediate disorder (Fig. 1(b)), and high disorder (Fig. 1(c)). Green stars are sketched to represent different disorder levels for illustrative purpose (not to scale). In our theoretical model, disorder is introduced as on-site potential fluctuations within the nanowire junction, denoted as $\delta U_i \in [-U_{\text{dis}}, U_{\text{dis}}]$. δU_i is the disorder potential at site i , randomly generated within the range $[-U_{\text{dis}}, U_{\text{dis}}]$. The disorder strength is defined by U_{dis} . Transport for each disorder distribution was calculated using the software package Kwant [49], see Supplemental Materials (SM) for details.

In the clean or low disorder regime, we set $U_{\text{dis}} = 0$. The calculated G_N and G_S are shown in the lower panel of Fig. 1(a), with G_S obtained by setting the bias to zero. Both G_N and G_S exhibit quantized plateaus. The Andreev doubling, where $G_S = 2G_N$ on the plateau, is also revealed.

In the intermediate disorder regime (Fig. 1(b)), we set U_{dis} to 14 meV. The G_N plateau at $2e^2/h$ remains, while the G_S plateau is destroyed and accompanied by a characteristic dip (indicated by the red arrow) induced by mode mixing. This dip feature typically appears on the right side of the G_N plateau where the second channel begins to be occupied. Assuming the normal-state transmissions of the first two channels are T_1 and T_2 , then $G_N = (T_1 + T_2) \times 2e^2/h$, and $G_S = [2T_1^2/(2 - T_1)^2 + 2T_2^2/(2 - T_2)^2] \times 2e^2/h$ [31, 33]. When only the first channel is occupied, $T_2 = 0$. As the second channel starts to be occupied (the right side of the G_N plateau), T_2 increases and disorder-induced mode mixing becomes significant. This mixing barely affects the total transmission

($T_1 + T_2$), thus the G_N plateau remains stable. In contrast, G_S can be significantly modified (suppressed) by the redistribution of the transmissions between T_1 and T_2 , resulting the observed dip. The consistency between these simulations and previous observed transport phenomena suggests that the best-optimized III-V nanowires fall within this intermediate disorder regime [28–30].

Figure 1(c) shows the high disorder regime with $U_{\text{dis}} = 40$ meV. Zero-field quantization is absent in both G_S and G_N . The early nanowire experiments around 2012 fall within this category. For more simulations of different U_{dis} 's and distributions with different random on-site potentials, see Fig. S1 in SM.

Next, we present transport results of PbTe-Pb hybrid nanowires. Figures 2(a-b) are the scanning electron micrographs (SEMs) of two devices. The PbTe is false-colored blue, the superconductor Pb is violet, and contacts and gates (Ti/Au) are yellow. Growth details of these devices are provided in Ref. [45]. The fabrication process is identical to that in our previous works [45–48]. The contact regions on the nanowire have been etched to remove the CdTe capping layer, ensuring ohmic contacts. Measurements were conducted in a dilution fridge at a base temperature of less than 50 mK using a standard two-terminal circuit.

Figure 2(c) depicts the differential conductance $G \equiv dI/dV$ of device A as a function of bias voltage (V) and gate voltage (V_G). I is the current passing through the device. A series resistance, contributed by contact resistance (R_c) and the fridge filters, has been subtracted. For device A, $R_c = 620 \Omega$. For a waterfall plot of Fig. 2(c), see Fig. S2 in SM. The green dashed lines delineate a diamond shape, indicating the quantization of G_N . The black curve in Fig. 2(d) is a line cut at $V = 1.2$ mV (outside the gap), revealing the G_N plateaus. The size of the diamond is ~ 7.3 meV, which measures the sub-

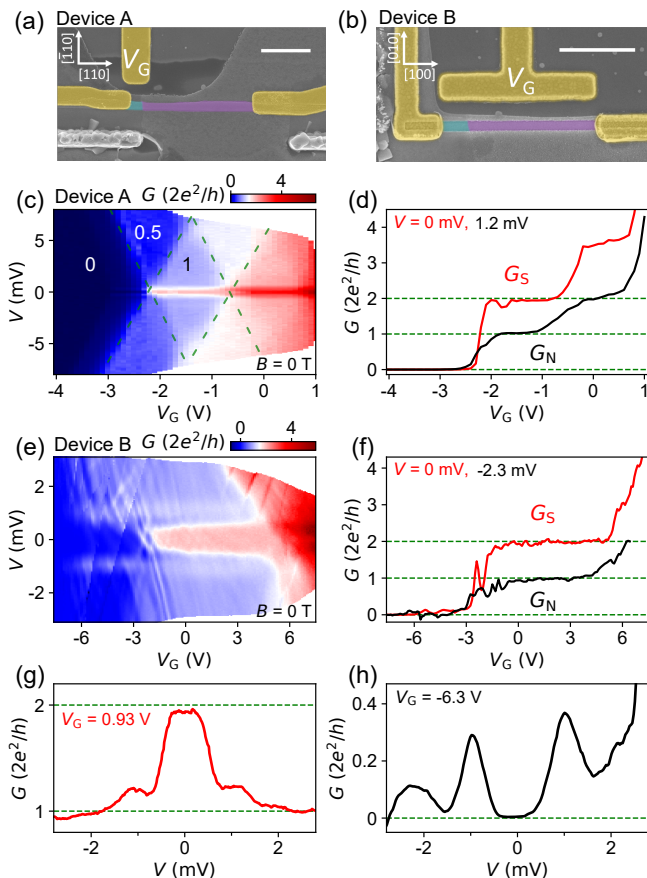


FIG. 2. Quantized Andreev conductance in PbTe-Pb nanowires at zero magnetic field. (a-b) False-colored SEM of two devices (A and B). Scale bars, 1 μm . (c) G vs V and V_G for device A. (d) Extracted G_S and G_N from (c). $V = 0$ mV and 1.2 mV, respectively. (e-f) Similar to (c-d) but for device B. (g-h) Line cuts from (e) in the open regime (on the G_N plateau) and tunneling regime. $V_G = 0.93$ V and -6.3 V, respectively.

band spacing. The labeled numbers represent the plateau values in units of $2e^2/h$. Within the $2e^2/h$ diamond, G near zero bias is significantly enhanced. The red curve in Fig. 2(d) shows the zero-bias line cut (G_S). G_S exhibits a plateau feature near $4e^2/h$, doubling the value of the G_N plateau. Notably, on the right side of the G_N plateau where the second channel starts to be occupied, G_S increases without dipping down, in sharp contrast to previous III-V experiments [28–30]. The absence of the dip feature suggests negligible mode mixing, indicating that the device has achieved the low disorder regime depicted in Fig. 1(a). The small dip on the left side of the plateau is likely charge instability. This is unlikely to be mode mixing, as the second channel is far from being occupied.

Figure 2(e) shows G vs V and V_G for device B, where $R_c = 560 \Omega$. The G_S and G_N line cuts are shown in Fig. 2(f), both exhibiting plateau features without the mode-mixing dip. Oscillations near pinch-off are observed in

G_S and G_N , which are likely Fabry-Pérot resonances. The visibility of Fabry-Pérot oscillations depends on the sharpness of the potential profiles within the wire. Even in clean wires, these oscillations are expected for a sharp potential profile (e.g. a square shape), and disappear for an adiabatically smoothed profile [50]. These oscillations occur near pinch-off and are thus not related to mode mixing, which occurs on the right side of the G_N plateau.

Figure 2(g) shows bias spectroscopy on the Andreev plateau (a vertical line cut of Fig. 2(e)). The outside-gap conductance is $\sim 2e^2/h$, corresponding to the G_N plateau. Near zero bias ($|V| < 0.4$ meV), G is enhanced/doubled to $4e^2/h$. Tuning the device into the tunneling regime (Fig. 2(h)), the subgap conductance is suppressed to zero, indicating a hard gap. The shoulders near $|V| \sim 1$ mV in Fig. 2(g) are likely related to the broad coherence peaks revealed in Fig. 2(h). The quality of the gap is moderate, as the coherence peaks are not sharply defined. The gap of device A in Fig. 2(c) is worse, i.e., smaller and softer (see Fig. S2 in SM for line cuts). These results indicate that the quantization of G_S and high-quality hard gap are not necessarily correlated.

We then investigate the magnetic field (B) dependence of the Andreev plateau. Figure 3(a) shows the B scan of device B with V fixed at 0 mV. B is roughly parallel to the wire axis. The $4e^2/h$ -Andreev plateau observed at zero field is suppressed and evolves into the $2e^2/h$ -normal plateau at high fields, see Fig. 3(b) for line cuts. For a continuous evolution, Fig. 3(c) shows a vertical line cut on the plateau region of Fig. 3(a). G_S drops sharply near 0.4 T, indicating a suppression of the induced superconductivity. The Fabry-Pérot resonances near pinch-off are barely affected by B . For line cuts at all fields, see Fig. S3 in SM.

The low critical field and broad coherence peaks are undesired in Majorana research and should be addressed in future optimizations. Although higher critical fields (> 2 T) can be achieved for some devices [41], the underlying mechanism of this device-to-device variation remains unclear. It might be related to the g -factor anisotropy in PbTe [38, 42], as a B parallel to the wire may induce a Zeeman splitting perpendicular to the wire direction [34]. Note that the superconducting gap is not protected if a Zeeman field is parallel to its spin-orbit direction [51]. Future optimization would require more systematic studies, such as exploring different wire geometries and symmetries. One possible solution for higher critical fields is to grow thinner wires to reduce the orbital effect [52, 53]. Another avenue worth exploring is the implementation of a uniform barrier layer, such as $\text{Pb}_{0.99}\text{Eu}_{0.01}\text{Te}$, inserted in between PbTe and Pb. This spacing layer is nearly lattice-matched with PbTe, thereby reducing the disorder caused by the mismatch between the superconductor and semiconductor.

The quantized Andreev conductance is observed not only in PbTe-Pb hybrids, but also in PbTe-In, as shown in Fig. 4. Figure 4(a) presents the SEM of a PbTe-In

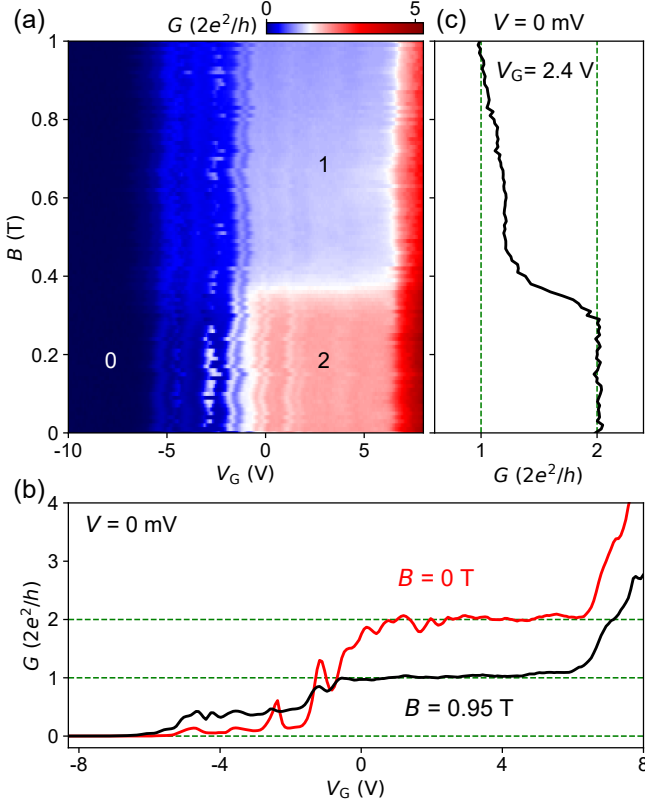


FIG. 3. B dependence of the Andreev conductance in device B. (a) G vs B and V_G . $V = 0$ mV. B is roughly aligned with the wire axis. The numbers label the plateau values in units of $2e^2/h$. (b) Line cuts at $B = 0$ T (red) and 0.95 T (black). (c) Line cut at $V_G = 2.4$ V, illustrating the continuous evolution of the G_S plateau.

nanowire. For the growth and transport characterization of PbTe-In hybrids, we refer to Ref. [46]. Figure 4(b) shows the 2D conductance map of the device depicted in Fig. 4(a) at zero magnetic field. $R_c = 1.4$ k Ω . The green dashed lines delineate the diamond shape corresponding to the G_N plateau, see the black curve in Fig. 4(d) for a line cut outside the gap. The red curve represents the conductance near zero bias (averaged over biases within 0.17 mV), revealing a quantized Andreev plateau around $4e^2/h$. The mode-mixing dip is also absent, indicating the low disorder regime.

Figure 4(c) shows the bias spectroscopy on the plateau, corresponding to a line cut at $V_{SG} = -0.92$ V. Within the superconducting gap ($|V| < 1$ mV), the conductance is enhanced to $4e^2/h$. Sizable oscillations are superimposed on the enhanced plateau, also visible as horizontal lines in Fig. 4(b). The origin is not fully unclear but might be related to Fabry-Pérot resonances. Outside the gap ($|V| > 1$ mV), the normal-state conductance exhibits a bias-dependent slope: it is slightly above $2e^2/h$ for positive V and below $2e^2/h$ for negative V . Figure S4 in SM shows the waterfall plot of this G_N asymmetry. Similar asymmetry has been observed in our previous devices

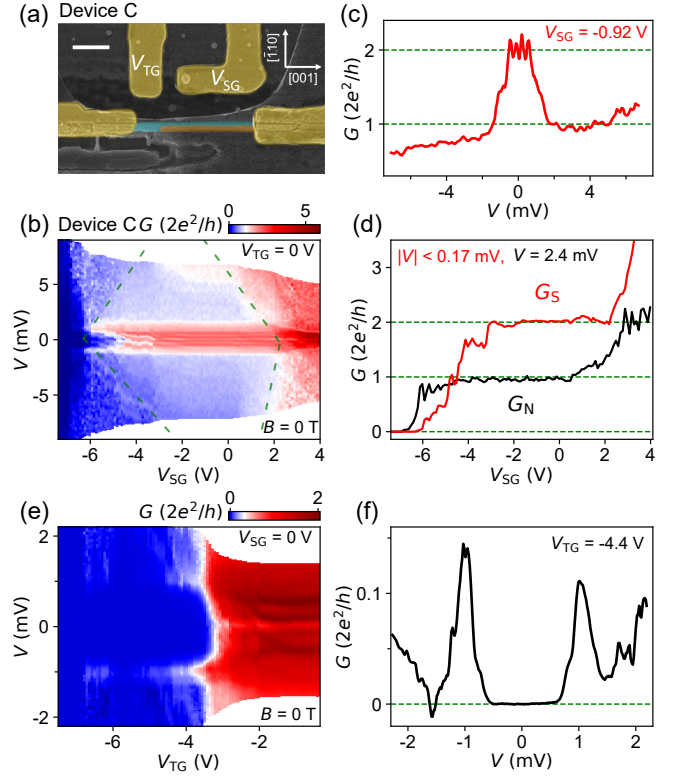


FIG. 4. Quantized Andreev conductance in a PbTe-In hybrid nanowire at $B = 0$ T. (a) Device SEM. Scale bar, 500 nm. The indium film on PbTe is false-colored orange. (b) G vs V and V_{SG} . $V_{TG} = 0$ V. (c) A vertical line cut from (b) on the plateau region. (d) Horizontal line cuts from (b), showing G_S and G_N ($V = 2.4$ mV). G_S is the average conductance within a bias window of $|V| < 0.17$ mV to eliminate the oscillation effect in (c). (e) Fine measurement in the tunneling regime. $V_{SG} = 0$ V. (f) A line cut from (e) at $V_{TG} = -4.4$ V.

[40–42], potentially related to the cross-talk between gate and bias voltages. Figure 4(e) is a fine scan over a smaller bias range, focusing on the tunneling regime to reveal the superconducting gap. A hard gap is observed, see Fig. 4(f) for a line cut. The gap size, ~ 1 meV, is consistent with our previous studies. The gap's critical field can reach 2 T, see Fig. S4 in SM.

In summary, we have observed quantized Andreev conductance in PbTe-Pb and PbTe-In hybrid nanowire devices. The absence of mode-mixing-induced dips suggests that our nanowires have reached the low disorder regime, which is unprecedented in comparison to previous studies on InAs and InSb nanowires. The observation indicates significant mitigation of disorder in PbTe nanowires, addressing a critical need in the field of Majorana research. These clean hybrid nanowires may facilitate better signatures in future explorations of Majorana zero modes. Future optimization efforts could focus on improving the device yield and enhancing the critical magnetic field.

Acknowledgment This work is supported by National Natural Science Foundation of China (92065206,

12374158, and 12074039) and the Innovation Program for Quantum Science and Technology (2021ZD0302400).

Raw data and processing codes within this paper are available at <https://doi.org/10.5281/zenodo.11895952>

-
- [1] R. M. Lutchyn, J. D. Sau, and S. Das Sarma, Majorana fermions and a topological phase transition in semiconductor-superconductor heterostructures, *Phys. Rev. Lett.* **105**, 077001 (2010).
- [2] Y. Oreg, G. Refael, and F. von Oppen, Helical liquids and Majorana bound states in quantum wires, *Phys. Rev. Lett.* **105**, 177002 (2010).
- [3] V. Mourik, K. Zuo, S. M. Frolov, S. Plissard, E. P. Bakkers, and L. P. Kouwenhoven, Signatures of Majorana fermions in hybrid superconductor-semiconductor nanowire devices, *Science* **336**, 1003 (2012).
- [4] M. Deng, S. Vaitiekėnas, E. B. Hansen, J. Danon, M. Leijnse, K. Flensberg, J. Nygård, P. Krogstrup, and C. M. Marcus, Majorana bound state in a coupled quantum-dot hybrid-nanowire system, *Science* **354**, 1557 (2016).
- [5] Ö. Gül, H. Zhang, J. D. Bommer, M. W. de Moor, D. Car, S. R. Plissard, E. P. Bakkers, A. Geresdi, K. Watanabe, T. Taniguchi, *et al.*, Ballistic Majorana nanowire devices, *Nature Nanotechnology* **13**, 192 (2018).
- [6] H. Song, Z. Zhang, D. Pan, D. Liu, Z. Wang, Z. Cao, L. Liu, L. Wen, D. Liao, R. Zhuo, *et al.*, Large zero bias peaks and dips in a four-terminal thin InAs-Al nanowire device, *Phys. Rev. Research* **4**, 033235 (2022).
- [7] Z. Wang, H. Song, D. Pan, Z. Zhang, W. Miao, R. Li, Z. Cao, G. Zhang, L. Liu, L. Wen, *et al.*, Plateau regions for zero-bias peaks within 5% of the quantized conductance value $2e^2/h$, *Phys. Rev. Lett.* **129**, 167702 (2022).
- [8] T. Dvir, G. Wang, N. van Loo, C.-X. Liu, G. Mazur, A. Bordin, S. Haaf, J.-Y. Wang, D. Driel, F. Zatelli, *et al.*, Realization of a minimal Kitaev chain in coupled quantum dots, *Nature* **614**, 445 (2023).
- [9] M. Aghaee, A. Akkala, Z. Alam, R. Ali, A. Alcaraz Ramirez, M. Andrzejczuk, A. E. Antipov, P. Aseev, M. Astafev, B. Bauer, *et al.* (Microsoft Quantum), InAs-Al hybrid devices passing the topological gap protocol, *Phys. Rev. B* **107**, 245423 (2023).
- [10] H. Zhang, D. E. Liu, M. Wimmer, and L. P. Kouwenhoven, Next steps of quantum transport in Majorana nanowire devices, *Nature Communications* **10**, 5128 (2019).
- [11] E. Prada, P. San-Jose, M. W. de Moor, A. Geresdi, E. J. Lee, J. Klinovaja, D. Loss, J. Nygård, R. Aguado, and L. P. Kouwenhoven, From Andreev to Majorana bound states in hybrid superconductor-semiconductor nanowires, *Nature Reviews Physics* **2**, 575 (2020).
- [12] W. Chang, S. Albrecht, T. Jespersen, F. Kuemmeth, P. Krogstrup, J. Nygård, and C. M. Marcus, Hard gap in epitaxial semiconductor-superconductor nanowires, *Nature Nanotechnology* **10**, 232 (2015).
- [13] P. Krogstrup, N. Ziino, W. Chang, S. Albrecht, M. Madsen, E. Johnson, J. Nygård, C. Marcus, and T. Jespersen, Epitaxy of semiconductor-superconductor nanowires, *Nature Materials* **14**, 400 (2015).
- [14] Ö. Gül, H. Zhang, F. K. de Vries, J. van Veen, K. Zuo, V. Mourik, S. Conesa-Boj, M. P. Nowak, D. J. van Woerkom, M. Quintero-Pérez, *et al.*, Hard superconducting gap in InSb nanowires, *Nano Letters* **17**, 2690 (2017).
- [15] D. Pan, H. Song, S. Zhang, L. Liu, L. Wen, D. Liao, R. Zhuo, Z. Wang, Z. Zhang, S. Yang, *et al.*, In situ epitaxy of pure phase ultra-thin InAs-Al nanowires for quantum devices, *Chinese Physics Letters* **39**, 058101 (2022).
- [16] J. Liu, A. C. Potter, K. T. Law, and P. A. Lee, Zero-bias peaks in the tunneling conductance of spin-orbit-coupled superconducting wires with and without Majorana end-states, *Phys. Rev. Lett.* **109**, 267002 (2012).
- [17] E. Prada, P. San-Jose, and R. Aguado, Transport spectroscopy of NS nanowire junctions with Majorana fermions, *Physical Review B* **86**, 180503 (2012).
- [18] D. Rainis, L. Trifunovic, J. Klinovaja, and D. Loss, Towards a realistic transport modeling in a superconducting nanowire with Majorana fermions, *Physical Review B* **87**, 024515 (2013).
- [19] C.-X. Liu, J. D. Sau, T. D. Stanescu, and S. D. Sarma, Andreev bound states versus Majorana bound states in quantum dot-nanowire-superconductor hybrid structures: Trivial versus topological zero-bias conductance peaks, *Physical Review B* **96**, 075161 (2017).
- [20] H. Pan and S. Das Sarma, Physical mechanisms for zero-bias conductance peaks in Majorana nanowires, *Phys. Rev. Research* **2**, 013377 (2020).
- [21] S. Ahn, H. Pan, B. Woods, T. D. Stanescu, and S. Das Sarma, Estimating disorder and its adverse effects in semiconductor majorana nanowires, *Phys. Rev. Materials* **5**, 124602 (2021).
- [22] S. Das Sarma and H. Pan, Disorder-induced zero-bias peaks in Majorana nanowires, *Phys. Rev. B* **103**, 195158 (2021).
- [23] C. Zeng, G. Sharma, S. Tewari, and T. Stanescu, Partially separated Majorana modes in a disordered medium, *Phys. Rev. B* **105**, 205122 (2022).
- [24] S. Das Sarma, J. D. Sau, and T. D. Stanescu, Spectral properties, topological patches, and effective phase diagrams of finite disordered Majorana nanowires, *Phys. Rev. B* **108**, 085416 (2023).
- [25] J. Kammerhuber, M. C. Cassidy, H. Zhang, Ö. Gül, F. Pei, M. W. de Moor, B. Nijholt, K. Watanabe, T. Taniguchi, D. Car, *et al.*, Conductance quantization at zero magnetic field in InSb nanowires, *Nano Letters* **16**, 3482 (2016).
- [26] J. Gooth, M. Borg, H. Schmid, V. Schaller, S. Wirths, K. Moselund, M. Luisier, S. Karg, and H. Riel, Ballistic one-dimensional InAs nanowire cross-junction interconnects, *Nano Letters* **17**, 2596–2602 (2017).
- [27] J. C. Estrada Saldana, Y.-M. Niquet, J.-P. Cleuziou, E. Lee, D. Car, S. Plissard, E. Bakkers, and S. Franceschi, Split-channel ballistic transport in an InSb nanowire, *Nano Letters* **18**, 2282 (2018).
- [28] H. Zhang, Ö. Gül, S. Conesa-Boj, M. P. Nowak, M. Wimmer, F. K. De Vries, J. Van Veen, M. W. De Moor, *et al.*, Ballistic superconductivity in semiconductor nanowires, *Nature Communications* **8**, 16025 (2017).
- [29] M. Kjaergaard, F. Nichele, H. Suominen, M. Nowak, M. Wimmer, A. Akhmerov, J. Folk, K. Flensberg, J. Shabani, C. Palmstrøm, and C. Marcus, Quantized con-

- ductance doubling and hard gap in a two-dimensional semiconductor-superconductor heterostructure, *Nature Communications* **7**, 12841 (2016).
- [30] S. Heedt, M. Quintero-Pérez, F. Borsoi, A. A. Fursina, N. van Loo, G. P. Mazur, M. P. Nowak, M. Ammerlaan, K. Li, S. Korneychuk, J. Shen, M. A. Y. van de Poll, G. Badawy, S. Gazibegović, N. de Jong, P. Aseev, K. van Hoogdalem, E. P. Bakkers, and L. P. Kouwenhoven, Shadow-wall lithography of ballistic superconductor–semiconductor quantum devices, *Nature Communications* **12** (2020).
- [31] G. E. Blonder, M. Tinkham, and T. M. Klapwijk, Transition from metallic to tunneling regimes in superconducting microconstrictions: Excess current, charge imbalance, and supercurrent conversion, *Phys. Rev. B* **25**, 4515 (1982).
- [32] M. Wimmer, A. Akhmerov, J. Dahlhaus, and C. Beenakker, Quantum point contact as a probe of a topological superconductor, *New Journal of Physics* **13**, 053016 (2011).
- [33] C. W. J. Beenakker, Quantum transport in semiconductor-superconductor microjunctions, *Phys. Rev. B* **46**, 12841 (1992).
- [34] Z. Cao, D. E. Liu, W.-X. He, X. Liu, K. He, and H. Zhang, Numerical study of PbTe-Pb hybrid nanowires for engineering Majorana zero modes, *Phys. Rev. B* **105**, 085424 (2022).
- [35] Y. Jiang, S. Yang, L. Li, W. Song, W. Miao, B. Tong, Z. Geng, Y. Gao, R. Li, F. Chen, Q. Zhang, F. Meng, L. Gu, K. Zhu, Y. Zang, R. Shang, Z. Cao, X. Feng, Q.-K. Xue, D. E. Liu, H. Zhang, and K. He, Selective area epitaxy of PbTe-Pb hybrid nanowires on a lattice-matched substrate, *Phys. Rev. Materials* **6**, 034205 (2022).
- [36] J. Jung, S. G. Schellingerhout, M. F. Ritter, S. C. ten Kate, O. A. van der Molen, S. de Loijer, M. A. Verheijen, H. Riel, F. Nichele, and E. P. Bakkers, Selective area growth of PbTe nanowire networks on InP, *Advanced Functional Materials* **32**, 2208974 (2022).
- [37] Z. Geng, Z. Zhang, F. Chen, S. Yang, Y. Jiang, Y. Gao, B. Tong, W. Song, W. Miao, R. Li, Y. Wang, Q. Zhang, F. Meng, L. Gu, K. Zhu, Y. Zang, L. Li, R. Shang, X. Feng, Q.-K. Xue, K. He, and H. Zhang, Observation of Aharonov-Bohm effect in PbTe nanowire networks, *Phys. Rev. B* **105**, L241112 (2022).
- [38] S. C. ten Kate, M. F. Ritter, A. Fuhrer, J. Jung, S. G. Schellingerhout, E. P. A. M. Bakkers, H. Riel, and F. Nichele, Small charging energies and g-factor anisotropy in PbTe quantum dots, *Nano Letters* **22**, 7049 (2022).
- [39] Z. Zhang, W. Song, Y. Gao, Y. Wang, Z. Yu, S. Yang, Y. Jiang, W. Miao, R. Li, F. Chen, Z. Geng, Q. Zhang, F. Meng, T. Lin, L. Gu, K. Zhu, Y. Zang, L. Li, R. Shang, X. Feng, Q.-K. Xue, K. He, and H. Zhang, Proximity effect in PbTe-Pb hybrid nanowire Josephson junctions, *Phys. Rev. Mater.* **7**, 086201 (2023).
- [40] W. Song, Y. Wang, W. Miao, Z. Yu, Y. Gao, R. Li, S. Yang, F. Chen, Z. Geng, Z. Zhang, S. Zhang, Y. Zang, Z. Cao, D. E. Liu, R. Shang, X. Feng, L. Li, Q.-K. Xue, K. He, and H. Zhang, Conductance quantization in PbTe nanowires, *Phys. Rev. B* **108**, 045426 (2023).
- [41] Y. Gao, W. Song, S. Yang, Z. Yu, R. Li, W. Miao, Y. Wang, F. Chen, Z. Geng, L. Yang, Z. Xia, X. Feng, Y. Zang, L. Li, R. Shang, Q.-K. Xue, K. He, and H. Zhang, Hard superconducting gap in PbTe nanowires, *Chinese Physics Letters* **41**, 038502 (2024).
- [42] Y. Wang, F. Chen, W. Song, Z. Geng, Z. Yu, L. Yang, Y. Gao, R. Li, S. Yang, W. Miao, W. Xu, Z. Wang, Z. Xia, H.-D. Song, X. Feng, T. Wang, Y. Zang, L. Li, R. Shang, Q. Xue, K. He, and H. Zhang, Ballistic PbTe nanowire devices, *Nano Letters* **23**, 11137 (2023).
- [43] R. Li, W. Song, W. Miao, Z. Yu, Z. Wang, S. Yang, Y. Gao, Y. Wang, F. Chen, Z. Geng, L. Yang, J. Xu, X. Feng, T. Wang, Y. Zang, L. Li, R. Shang, Q. Xue, K. He, and H. Zhang, Selective-area-grown PbTe-Pb planar Josephson junctions for quantum devices, *Nano Letters* **24**, 4658 (2024).
- [44] M. Gupta, V. Khade, C. Riggert, L. Shani, G. Menning, P. Lueb, J. Jung, R. Melin, E. P. A. M. Bakkers, and V. S. Pribiag, Evidence for π -shifted Cooper quartets in PbTe nanowire three-terminal Josephson junctions, arXiv: 2312.17703 (2023).
- [45] W. Song *et al.*, Reducing disorder in PbTe nanowires for Majorana research, arXiv: 2402.02132 (2024).
- [46] Z. Geng *et al.*, Epitaxial Indium on PbTe nanowires for quantum devices, arXiv: 2402.04024 (2024).
- [47] Y. Wang *et al.*, Gate-tunable subband degeneracy in semiconductor nanowires, arXiv: 2404.02760 (2024), 2404.02760.
- [48] Y. Gao *et al.*, Squid oscillations in PbTe nanowire networks, arXiv: 2404.06899 (2024), 2404.06899.
- [49] C. W. Groth, M. Wimmer, A. R. Akhmerov, and X. Waintal, Kwant: a software package for quantum transport, *New Journal of Physics* **16**, 063065 (2014).
- [50] F. A. Maaß, I. V. Zozulenko, and E. H. Hauge, Quantum point contacts with smooth geometries: Exact versus approximate results, *Phys. Rev. B* **50**, 17320 (1994).
- [51] J. D. Bommer, H. Zhang, Ö. Gül, B. Nijholt, M. Wimmer, F. N. Rybakov, J. Garaud, D. Rodic, E. Babaev, M. Troyer, *et al.*, Spin-orbit protection of induced superconductivity in Majorana nanowires, *Physical Review Letters* **122**, 187702 (2019).
- [52] B. Nijholt and A. R. Akhmerov, Orbital effect of magnetic field on the Majorana phase diagram, *Phys. Rev. B* **93**, 235434 (2016).
- [53] O. Dmytruk and J. Klinovaja, Suppression of the overlap between Majorana fermions by orbital magnetic effects in semiconducting-superconducting nanowires, *Phys. Rev. B* **97**, 155409 (2018).

Supplemental Material for “Quantized Andreev conductance in semiconductor nanowires”

Yichun Gao,^{1,*} Wenyu Song,^{1,*} Yuhao Wang,^{1,*} Zuhan Geng,^{1,*} Zhan Cao,^{2,*} Zehao Yu,¹ Shuai Yang,¹ Jiaye Xu,¹ Fangting Chen,¹ Zonglin Li,¹ Ruidong Li,¹ Lining Yang,¹ Zhaoyu Wang,¹ Shan Zhang,¹ Xiao Feng,^{1,2,3,4} Tiantian Wang,^{2,4} Yunyi Zang,^{2,4} Lin Li,² Dong E. Liu,^{1,2,3,4} Runan Shang,^{2,4} Qi-Kun Xue,^{1,2,3,4,5} Ke He,^{1,2,3,4,†} and Hao Zhang^{1,2,3,‡}

¹*State Key Laboratory of Low Dimensional Quantum Physics,*

Department of Physics, Tsinghua University, Beijing 100084, China

²*Beijing Academy of Quantum Information Sciences, Beijing 100193, China*

³*Frontier Science Center for Quantum Information, Beijing 100084, China*

⁴*Hefei National Laboratory, Hefei 230088, China*

⁵*Southern University of Science and Technology, Shenzhen 518055, China*

Details of numerical simulations

We simulate the disorder effect using a two-dimensional effective Hamiltonian:

$$H = \left[\frac{p_x^2 + p_y^2}{2m_{eff}} - \mu + V_{QPC}(x) + V_{dis}(x, y) \right] \tau_3 + \Delta(x) \tau_1, \quad (1)$$

with m_{eff} the effective electron mass, $p_{x(y)}$ the momentum operator, μ the chemical potential, $V_{QPC}(x)$ the electrostatic potential forming the quantum point contact (QPC) region, $V_{dis}(x, y)$ the disorder-induced potential landscape, Δ the superconducting pairing potential, and $\tau_{1(3)}$ the Pauli matrix acting on the electron-hole degree of freedom. x -axis refers to the longitudinal direction of the wire ($-\infty < x < \infty$), and y -axis refers to the transverse direction ($-W/2 < y < W/2$) (W defines the wire width). The QPC, formed within the range of $-d/2 < x < d/2$, is contacted to a normal lead on the left side of the wire and to a superconducting lead [$\Delta(x) = \Delta_0 \theta(x - d/2)$] on the right side of the wire. G_N is calculated by setting [$\Delta(x) = 0$]. We neglect spin-orbit coupling and Zeeman energy, and solely focus on the effect of disorder.

For simplicity, we employ a symmetric smooth QPC potential

$$V_{QPC}(x) = -\frac{eU_{QPC}}{2} \left(\tanh \frac{x + w/2}{\lambda} - \tanh \frac{x - w/2}{\lambda} \right), \quad (2)$$

where U_{QPC} , w , and λ model the height, width, and smoothness, respectively. V_{QPC} approaches eU_{QPC} for $|x| < w/2$ and zero for $|x| > w/2 + \lambda$. We assume $d = 200$ nm, $w = 45$ nm, and $\lambda = 10$ nm. U_{QPC} varies from -40 meV to 0 meV to simulate the effect of a gate voltage, i.e. the x -axis of the simulation plots in Fig. 1 and Fig. S1. In the QPC region, the spatially varying disorder potential $V_{dis}(x, y)$ is modeled by random numbers obeying the uniform distribution within the range $[-U_{dis}, U_{dis}]$. Note that the model is not completely identical to the actual device, as the nanowire in the actual device has a finite length and is contacted by source/drain metal leads (while in the model it is infinitely long without metal leads). To account for this difference, the disorder potential is introduced only in the QPC region.

We focus on the zero-bias conductance at zero temperature, which can be calculated by the scattering matrix formalism [1]:

$$G = \frac{e^2}{h} \text{Tr} \left[I - |S_{ee}(0)|^2 + |S_{he}(0)|^2 \right]. \quad (3)$$

The scattering matrix $S_{ee}(0)$ and $S_{he}(0)$ are associated with the normal and Andreev reflections, respectively, of electrons at the Fermi level (i.e., $E = 0$). They can be readily obtained with the Kwant package [2] by discretizing the Hamiltonian (1) on a square lattice with a spacing of a . In all simulations, we adopt the parameters $m_{eff} = 0.04 m_e$ (m_e is the free electron mass), $W = 40$ nm, $\mu = 30$ meV, $\Delta_0 = 0.4$ meV, and $a = 2$ nm.

* equal contribution

† kehe@tsinghua.edu.cn

‡ hzquantum@mail.tsinghua.edu.cn

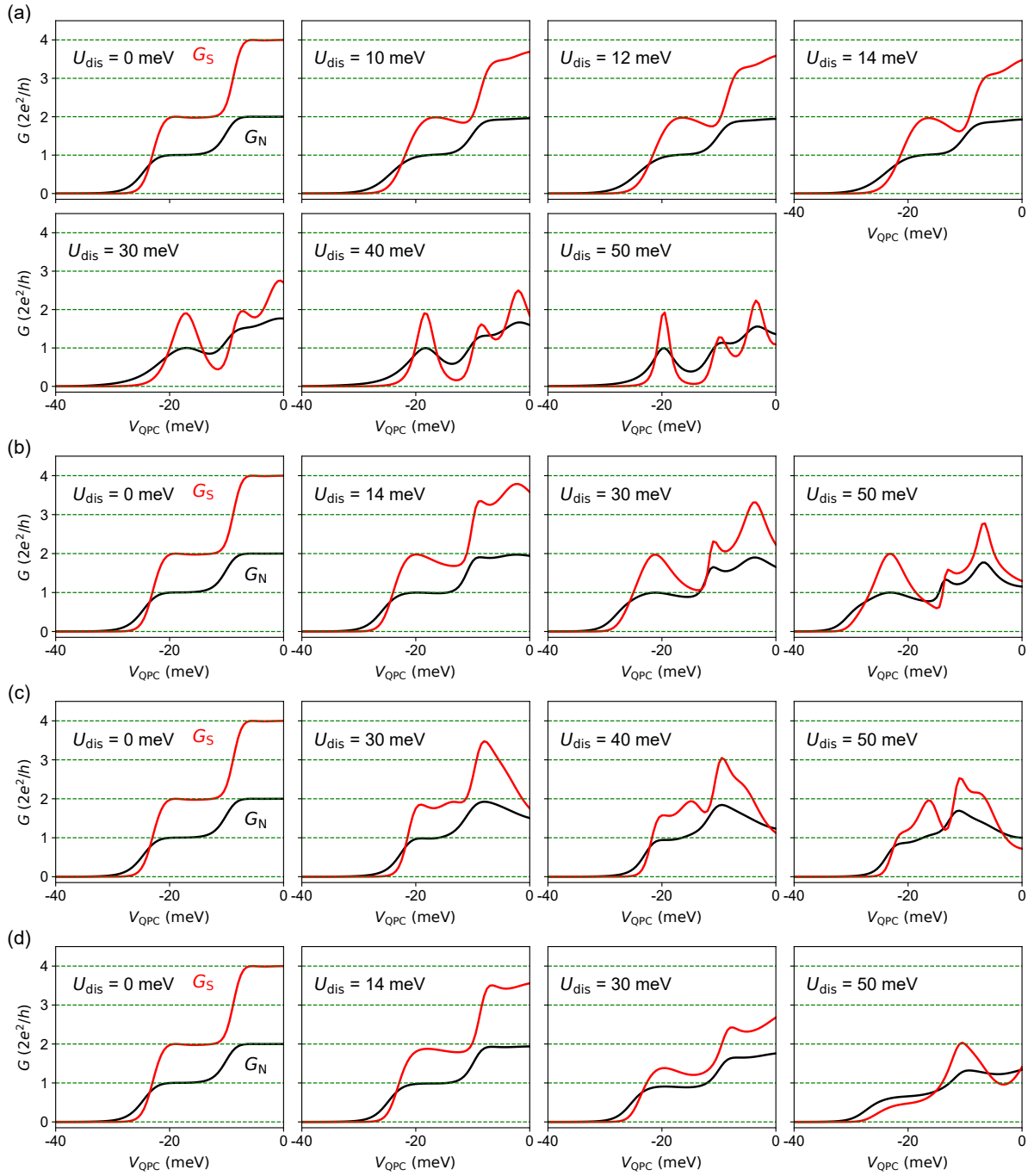


FIG. S1. Additional simulations. (a) Disorder distribution same with that in Fig. 1. We first generated $\delta U_i \in [-1 \text{ meV}, 1 \text{ meV}]$, and then scaled δU_i by a factor of 0, 10, 12, 14, 30, 40, and 50 to obtain the transport behaviors shown in the 5 panels, respectively. The 0, 14, and 40 meV cases have been shown in Fig. 1. (b-d) Another three random distributions of δU_i , showing similar behavior. The Andreev plateau is in general more sensitive to disorder than the normal-state plateau.

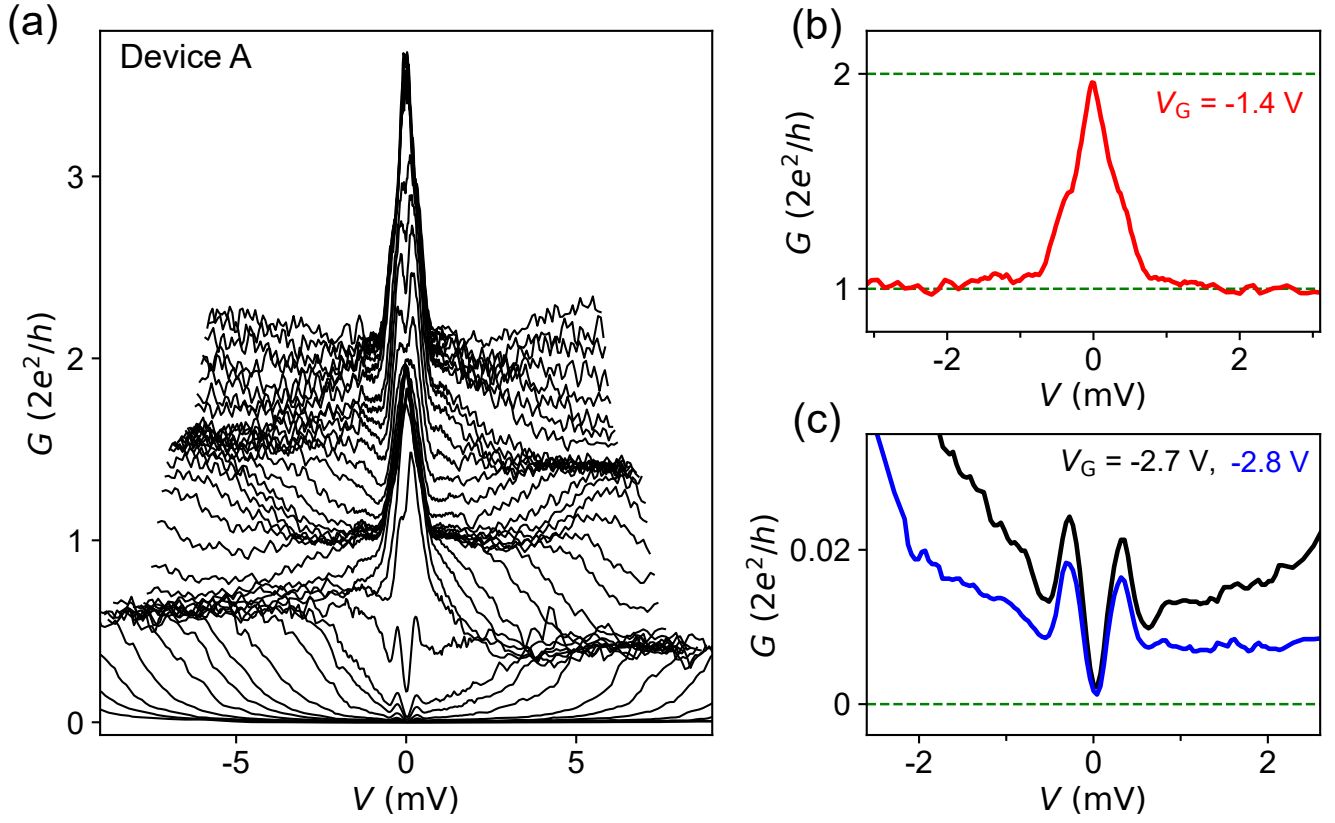


FIG. S2. (a) Waterfall plot of Fig. 2(c). The gate voltage range is from -3.5 V to 0.4 V for clarity. Plateaus are revealed as clusters of line cuts. At low biases (outside the gap), the $2e^2/h$ plateau is observable, while half plateaus (near $0.5 \times 2e^2/h$ and $1.5 \times 2e^2/h$) can be revealed at higher biases. (b) Bias scan on the plateau, corresponding to a line cut at $V_G = -1.4$ V. The outside gap conductance reaches the $2e^2/h$ normal plateau, the zero-bias conductance is close to $4e^2/h$. (c) Bias scan in the tunneling regimes, resolving a soft gap.

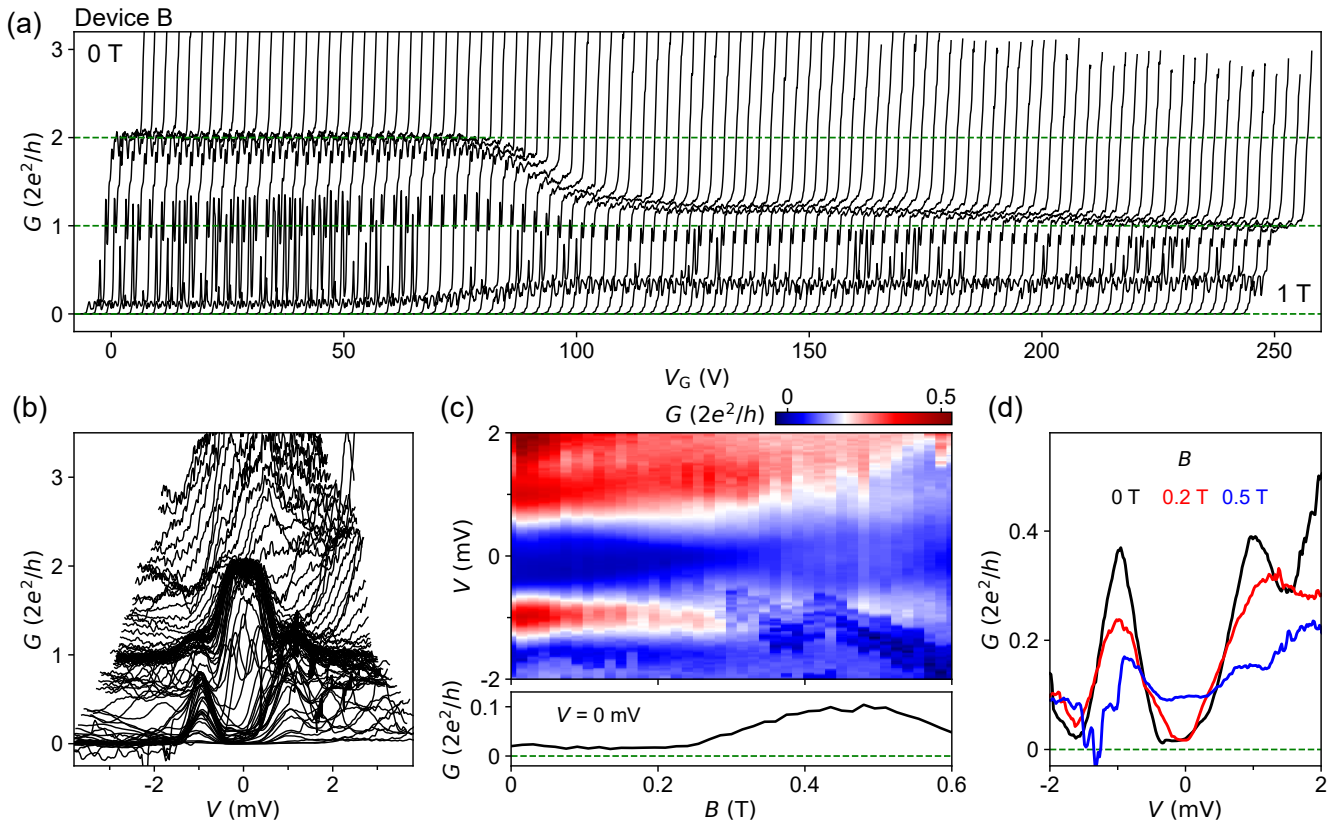


FIG. S3. (a) All line cuts of Fig. 3(a), illustrating the gradual evolution of the Andreev plateau in B . Horizontal offset between neighboring curves is 2.5 V for clarity. (b) Waterfall plot of Fig. 2(e), showing the $4e^2/h$ Andreev plateau and $2e^2/h$ normal plateau as clusters of line cuts. (c) B dependence of the gap. B is parallel to the wire axis. Lower panel, zero-bias line cut. The gap closes around 0.4 T, consistent with the transition field of the Andreev plateau shown in Fig. 3(a). (d) Line cuts from (c) at different fields.

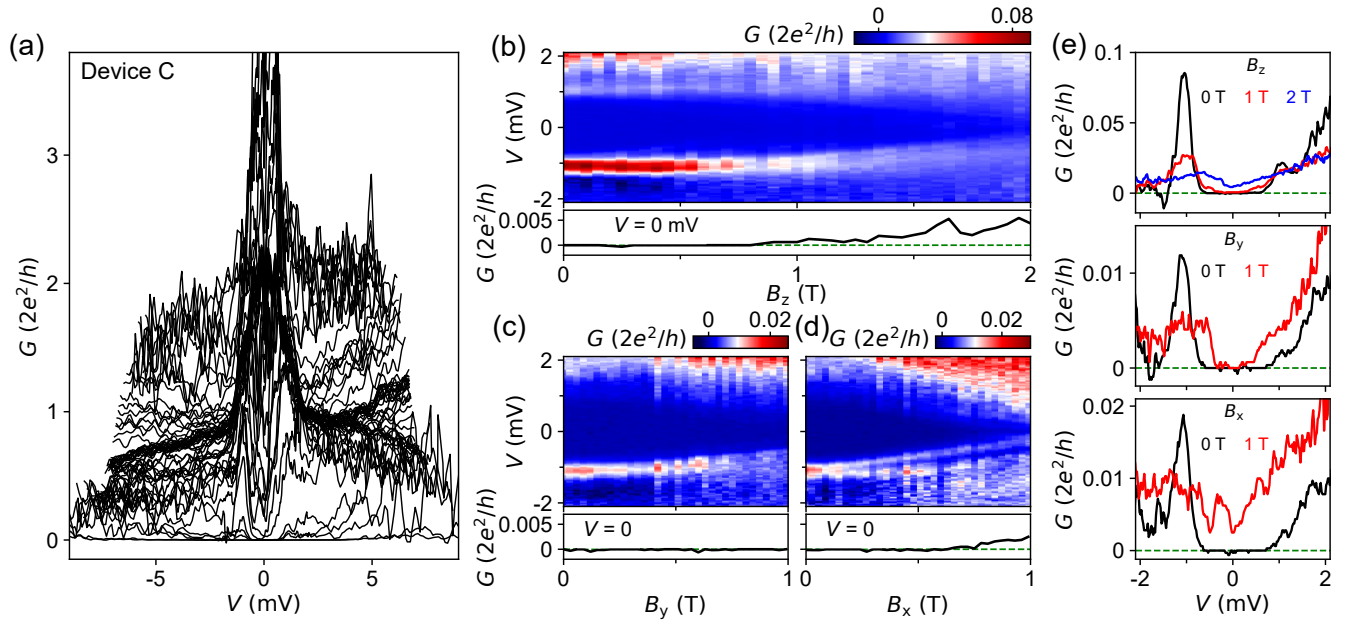


FIG. S4. (a) Waterfall plot of Fig. 4(b). (b-d) B dependence of the gap along three axis. B_z is parallel to the wire, B_x is perpendicular to the wire and in-plane, B_y is out of plane. Lower panels are zero-bias line cuts. (e) Line cuts at different fields. The critical field along the z axis is near 2 T.

-
- [1] G. E. Blonder, M. Tinkham, and T. M. Klapwijk, Transition from metallic to tunneling regimes in superconducting micro-constrictions: Excess current, charge imbalance, and supercurrent conversion, *Phys. Rev. B* **25**, 4515 (1982).
 [2] C. W. Groth, M. Wimmer, A. R. Akhmerov, and X. Waintal, Kwant: a software package for quantum transport, *New Journal of Physics* **16**, 063065 (2014).